ACS APPLIED MATERIALS & INTERFACES

Research Article

Cite This: ACS Appl. Mater. Interfaces 2019, 11, 5536−5543

www.acsami.org

Strain-Induced Metastable Phase Stabilization in Ga_2O_3 Thin Films

Yaobin Xu,[†,‡] Ji-Hyeon Park,[§] Zhenpeng Yao,[†,⊥] Chris Wolverton,[†] Manijeh Razeghi,[§] Jinsong Wu,[*,†,‡,∥] and Vinayak P. Dravid[*,†,‡]

[†]Department of Materials Science and Engineering, [‡]NUANCE Center, and [§]Center for Quantum Devices, Department of Electrical Engineering and Computer Science, Northwestern University, Evanston, Illinois 60208, United States

Supporting Information

ABSTRACT: It is well known that metastable and transient structures in bulk can be stabilized in thin films via epitaxial strain (heteroepitaxy) and appropriate growth conditions that are often far from equilibrium. However, the mechanism of heteroepitaxy, particularly how the nominally unstable or metastable phase gets stabilized, remains largely unclear. This is especially intriguing for thin-film Ga_2O_3, where multiple crystal phases may exist under varied growth conditions with spatial and dimensional constraints. Herein, the development and distribution of epitaxial strain at the Ga_2O_3/Al_2O_3 film−substrate interfaces is revealed down to the atomic resolution along different orientations, with an aberration-corrected scanning transmission electron microscope. Just a few layers of metastable α-Ga_2O_3 structure were found to accommodate the misfit strain in direct contact with the substrate. Following an epitaxial α-Ga_2O_3 structure of about couple unit cells, several layers (4−5) of transient phase appear as the intermediate structure to release the misfit strain. Subsequent to this transient crystal phase, the nominally unstable κ-Ga_2O_3 phase is stabilized as the major thin-film phase form. We show that the epitaxial strain is gracefully accommodated by rearrangement of the oxygen polyhedra. When the structure is under large compressive strain, Ga^{3+} ions occupy only the oxygen octahedral sites to form a dense structure. With gradual release of the compressive strain, more and more Ga^{3+} ions occupy the oxygen tetrahedral sites, leading to volumetric expansion and the phase transformation. The structure of the transition phase is identified by high-resolution electron microscopy observation, complemented by the density functional theory calculations. This study provides insights from the atomic scale and their implications for the design of functional thin-film materials using epitaxial engineering.

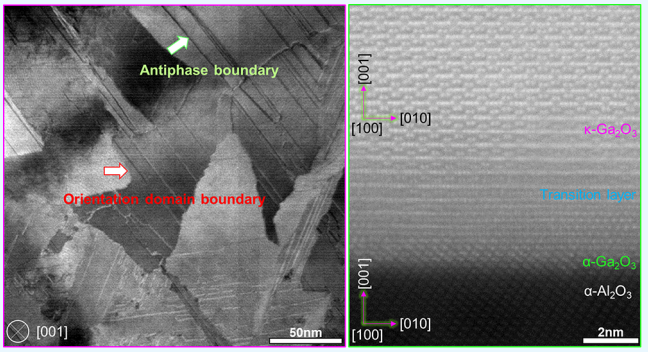

KEYWORDS: *κ-Ga_2O_3, α-Ga_2O_3, metastable phase, misfit strain, aberration-corrected scanning transmission electron microscopy*

INTRODUCTION

Epitaxial growth of thin films on dissimilar substrates has been extensively studied for decades, and the need for structural resemblance between the film and the substrate is widely noticed and accepted.[1−4] It is also known that due to constraints imposed by the substrate, many unstable, metastable, and unusual polymorphs can appear in the thin-film phases, often termed epitaxial stabilization. These epitaxial stabilization phenomena are mostly explained by free energy minimization, in which the energy of coherent and semi-coherent interfaces is significantly lower than that of noncoherent ones.[2] Thus, the formation of low-energy interfaces and the minimization of overall free energy of the system (e.g., due to volume strain energy contribution) often lead to stabilization of otherwise unstable, metastable, or nonequilibrium structures. Although free energy minimization provides a perfect albeit generic explanation, a critical structural view that permits the understanding of the mechanisms of epitaxial stabilization, particularly the impact of the substrate on the structure of interface and thin-film phases at atomic resolution, is still evolving.

Epitaxial stabilization can be used as an effective tool of solid state chemistry to construct special structures of interest, even if they are unstable (metastable, nonequilibrium) as a bulk material. Indeed, many unstable structures that must be synthesized in severe conditions in the bulk state (e.g., high pressure, highly oxidative environment, high temperature) can be realized in gentler conditions, using epitaxial stabilization to form useful thin-film phases. To develop the epitaxial stabilization into a useful tool for materials synthesis, more details on the mechanisms of epitaxial stabilization, i.e., how the substrate, misfit between the substrate and thin film, temperature, etc. affect the structure of thin films, must be further explored. When the epitaxial stabilization phenomenon can be understood at the nanometer and even atomic scale, it

Received: October 20, 2018
Accepted: January 10, 2019
Published: January 10, 2019

DOI: 10.1021/acsami.8b17731
ACS Appl. Mater. Interfaces 2019, 11, 5536−5543

Table 1. Crystallographic Data of Ga_2O_3 Polymorphs

phase	space group	lattice parameter	ref
α	$R\bar{3}c$	a = 0.4983 nm, c = 1.3433 nm	8
β	$C2/m$	a = 1.2214 nm, b = 0.3037 nm, c = 0.5798 nm, β = 103.83°	9
γ	$Fd\bar{3}m$	a = 0.822 nm	10
ε	$P6_3mc$	a = 0.2904 nm, c = 0.9255 nm	6
δ	$la3$	a = 0.952 nm	11
κ	$Pna2_1$	a = 0.512 nm, b = 0.8792 nm, c = 0.941 nm	12

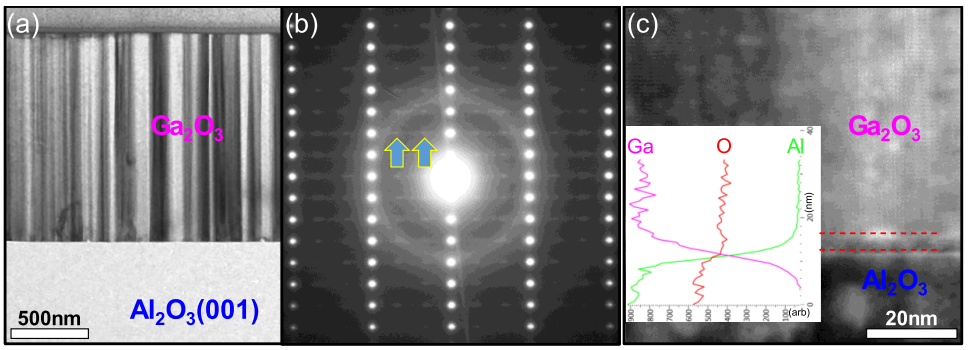

Figure 1. (a) Bright-field TEM image showing the typical morphology of Ga_2O_3/Al_2O_3 film system. Note that the film has a high density of planar defects. (b) SAED from film has shown extra spot as indicated by blue arrows and the line contrast along the interface direction. (c) Cross-sectional BF-STEM image showing the Ga_2O_3 film, the interfacial layer, and the Al_2O_3 substrate; inset is EDS line-scan profiles scanned perpendicular to the interface, which indicates that the interfacial layer is mainly composed of Ga and O.

can be better designed as an engineering tool to synthesize novel structures with unique and improved properties.

In this work, using Ga_2O_3 as the test case of thin-film sample, we have designed a scheme to grow the nominally unstable κ-Ga_2O_3 phase, identified the thin-film phases, and studied the interface structure using electron microscopy at atomic resolution to disclose the mechanism of epitaxial stabilization.

Gallium oxide (Ga_2O_3) has attracted considerable interest as a functional material for various applications because of its advantageous physical properties.[5,6] Due to its large direct band gap (4.7−4.9 eV) and high breakdown voltage (8 MV cm^{-1}), which is considered the widest band gap semiconductor among transparent conducting oxides, it has been used in power and high voltage devices.[7] Because of its unique structural characteristics of coordinately unsaturated Ga^{3+} cations, Ga_2O_3 has a high catalytic activity for hydrocarbon activation in a CO_2 atmosphere.[4] In addition, it could be used as an optical limiter for deep ultraviolet radiation, solar energy conversion devices, Schottky diodes, field effect transistors, as well as photocatalyst and high-temperature stable gas sensors.[9−13]

Ga_2O_3 exhibits polymorphisms, similar to aluminum oxide.[5,14−16] Four Ga_2O_3 polymorphs can be found in the ICSD database, designated as α, β, γ, and ε phases.[14,17−19] Two other phases, δ and κ, have also been recently reported in the literature.[20,21] The space group and lattice parameters of the Ga_2O_3 polymorphs are listed in Table 1. Unlike the structures of alumina polymorphs, the structures of several of the gallium oxide (such as γ, δ, the relationship between κ and ε) polymorphs remain poorly understood.[15,16,22] As Ga_2O_3 polymorphs have different crystalline and electronic structures, they possess different physical properties. For example, the Ga_2O_3 polymorphs have quite different photocatalytic activities, and their specific activities increased in the following order: γ-Ga_2O_3 < α-Ga_2O_3 < β-Ga_2O_3.[10]

The α-Ga_2O_3 phase, similar to the α-Al_2O_3, has a corundum structure that contains only octahedrally (GaO_6) coordinated Ga^{3+} ion. It is metastable compared to its alumina analog but can be stabilized by low-temperature heteroepitaxial growth on sapphire substrates and converted to the β form at a temperature higher than 500 °C.[5] The monoclinic β-Ga_2O_3 phase is the only thermodynamically stable form of Ga_2O_3,[1212] which is analogous to θ-Al_2O_3, and contains equal proportion of octahedrally and tetrahedrally (GaO_4) coordinated gallium. The γ-Ga_2O_3 is analogous to γ-Al_2O_3 and has cation-deficient cubic spinel structure ($MgAl_2O_4$-type). In γ-Ga_2O_3, Ga^{3+} ions partially occupy both tetrahedral and octahedral sites. Playford et al. reported that ratio values of octahedral and tetrahedral were 1.8:1, 1.8:1, and 2.1:1 for the crystalline, nanocrystalline, and disordered samples of γ-Ga_2O_3, respectively.[23] The ε-Ga_2O_3 is the second most stable polymorph after β-Ga_2O_3, consisting of a 4H stacking of close-packed oxygen layers, in which the disordered Ga^{3+} ion distributed over three partially occupied sites, with an octahedral/tetrahedral ratio of 2.2:1.[16] Very few studies have been reported on the other metastable phases because of the difficulty in the synthesis of a single-phase crystal.

The properties of the Ga_2O_3 can be tuned by Ga^{3+}-occupied sites, for example, by adjusting the octahedral/tetrahedral ratio. It is known that the wave function of the conduction band bottom is composed mostly of 4s orbitals of Ga^{3+} ion in octahedral sites.[24] Meanwhile, the volume of the oxygen frame expands when there are more tetrahedrally occupied Ga-ions. Tensile strain in the thin film may lead to more Ga^{3+} ions in the tetrahedral sites, whereas compressive strain most likely leads to more octahedral occupancy of Ga^{3+} ions. One of the authors (M.R.) has developed elaborate procedure for high-quality growth of Ga_2O_3 thin films via heteroepitaxial metal organic chemical vapor deposition (MOCVD) method using H_2 as a carrier gas, on c-sapphire substrates, using trimethylgallium (TMGa) and water, as gallium and oxygen

DOI: 10.1021/acsami.8b17731
ACS Appl. Mater. Interfaces 2019, 11, 5536−5543

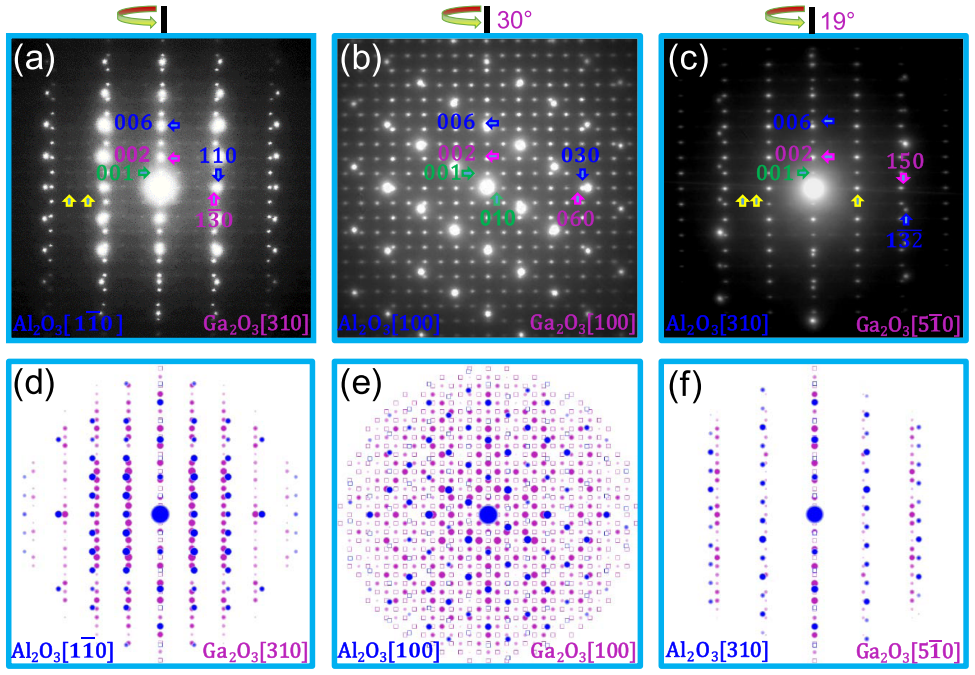

Figure 2. Series of EDPs of the Ga_2O_3/Al_2O_3 film system obtained by a large-angle tilting of the crystal: (a) $[1\bar{1}0]$; (b) [100]; (c) [310] zone axis of Al_2O_3 EDPs. κ-Ga_2O_3 with the space group $Pna2_1$ is identified by the EDPs. Related simulated electron diffraction patterns of (d) $Al_2O_3[1\bar{1}0]$ and κ-Ga_2O_3[310]; (e) Al_2O_3[100] and κ-Ga_2O_3[100]; (f) Al_2O_3[310] and κ-$Ga_2O_3[5\bar{1}0]$, which are consistent with experimental results of (a), (b), and (c). Yellow arrows indicating extra diffraction spots are related to the planar defects. Green arrows indicating extra diffraction spots are proposed to result from double diffraction.

precursors, respectively. The details of growth conditions and related information are reported in an earlier publication.[25]

We have utilized (scanning) transmission electron microscopy ((S)TEM) complemented by density functional theory (DFT) calculations, to investigate the structure of Ga_2O_3 thin films on Al_2O_3(001) substrate, to identify the various Ga_2O_3 thin-film phases, and to explore the mechanism of epitaxial stabilization. We believe that such a comprehensive approach may pave the way for epitaxial engineering to synthesize other related novel materials and structures.

RESULTS AND DISCUSSION

Figure 1a is a cross-sectional bright-field (BF) TEM image showing the typical morphology of the Ga_2O_3/Al_2O_3(001) film system. The film has a uniform thickness of about 1280 nm. The surface of the Ga_2O_3 film is quite flat without terraces or fluctuations. The film exhibits high-density, line-like contrast threading the whole film. However, along the interface there are no obvious defects that can be observed. From the selected area electron diffraction (SAED) pattern of the Ga_2O_3 film as shown in Figure 1b, many structural characters of the film can be figured out. There are extra and periodic weak spots as labeled by the blue arrow-heads indicating that a certain type of ordered superstructure occurred along the interface direction. Meanwhile, in the pattern there are also diffused lines along the interface direction, which indicates that the ordered superstructure has many planar defects along this direction. The Figure 1c is a low-magnification cross-sectional BF-STEM image taken along the [100] direction of Al_2O_3 showing the interface of the Ga_2O_3/Al_2O_3(001) film system. It is evident that the uniform interfacial/transitional layer is formed between the Ga_2O_3 and the Al_2O_3 substrate. The thickness of this interfacial layer is about 4 nm. The compositional variations of the thin film and interface are analyzed by energy-dispersive spectrometer (EDS), as shown in the inset of Figure 1c. It was determined that the interfacial layer was mainly composed of Ga and O, similar to the thin-film phase.

The major Ga_2O_3 thin-film phase is identified as κ-Ga_2O_3, which is an analog of orthorhombic κ-Al_2O_3 with the space group of $Pna2_1$. Ga_2O_3 has several polymorphs and among them κ phase structure is similar to ε phase. As shown in Figure S1, κ phase and ε phase have similar two-dimensional diffraction patterns along some zone axis. So, here a series of electron diffraction patterns (EDPs) obtained by a large-angle tilting of the thin film as shown in Figures 2a–c and S2b–d are used to identify the structure of Ga_2O_3 film. Compared to the simulated EDPs as shown in Figures 2d–f and S2e–g, κ phase is identified as the patterns match well to each other as well as the tiling angles. Diffraction spots indicated by green arrows are from double diffraction, which complies well with reflection conditions of the space group of $Pna2_1$. Meanwhile, there were also other extra electron diffraction spots as indicated by yellow arrows in Figure 2a–f, implying that there exists a certain type of ordering in the structure which is a rotational domain structure (discussed in the following section). No extra spots could be observed except those from the film, substrate, and superstructure, indicating that the films were free of secondary phase. Meanwhile, no diffraction spots from the interfacial layer could be observed because of its low volume fraction. It is evident that by the MOCVD method, we have successfully synthesized a stable κ-Ga_2O_3 film phase, which was considered an unstable phase in Ga_2O_3 polymorph.[16] In addition, a closed orientation relationship can be derived from the electron diffraction patterns: $[310]_{\kappa\text{-}Ga_2O_3}//[1\bar{1}0]_{Al_2O_3}$, $(004)_{\kappa\text{-}Ga_2O_3}//(006)_{Al_2O_3}$, and $[1\bar{3}0]_{\kappa\text{-}Ga_2O_3}//(110)_{Al_2O_3}$. Those orientation relationships can be illustrated by a matrix, as

DOI: 10.1021/acsami.8b17731
ACS Appl. Mater. Interfaces 2019, 11, 5536–5543

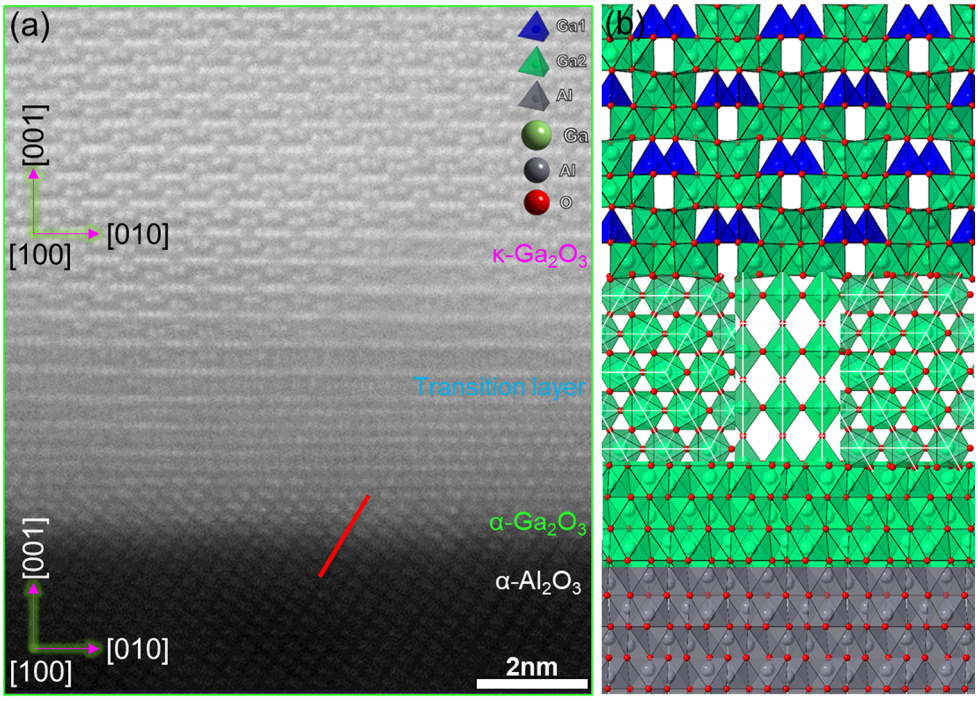

Figure 3. (a) Cross-sectional aberration-corrected STEM images of the Ga_2O_3/Al_2O_3 interface viewed along the $[100]_{\kappa\text{-}Ga_2O_3}$ zone axis. (b) Atomic illustration of the interface structure consisting of the α-Al_2O_3 substrate, α-Ga_2O_3 layer, cubic Ga_2O_3 intermediate layer, and κ-Ga_2O_3. The Ga^{3+} ions in blue are tetrahedrally coordinated, whereas the Ga^{3+} ions in green are octahedral sites.

Table 2. Calculated Three-Dimensional Lattice Mismatch Among the Substrate (α-Al_2O_3), α-Ga_2O_3, and κ-Ga_2O_3[a]

				f (misfit match)		
phase	α-Al_2O_3 (Å)	α-Ga_2O_3 (Å)	κ-Ga_2O_3 (Å)	12 (%)	23 (%)	13 (%)
in-plane	$3\bar{3}0$; 1.374	$3\bar{3}0$; 1.437	310; 1.675	−4.48	−15.30	−19.74
in-plane	110; 2.379	110; 2.490	130_T; 2.543	−4.56	−2.11	−6.66
			130_E; 2.520		−1.00	−5.56
in-plane	100; 4.121	100; 4.312	100; 5.120	−4.53	−17.13	−21.62
in-plane	010; 4.121	010; 4.312	020_T; 4.396	−4.53	−1.93	−6.46
			020_E; 4.346		−0.79	−5.31
out-of-plane	003; 4.331	003; 4.476	002_T; 4.705	−3.29	−4.99	−8.28
			002_E; 4.643		−3.66	−6.95

[a]In the table, theoretical values are labeled by "T" after the lattice plane index, whereas the experimental values are labeled by "E".

shown in Figure S3. Moreover, the splitting of high-order spots could be identified in Figure 2a,b, which were due to the difference in lattice constants of Al_2O_3 and κ-Ga_2O_3. The splitting of the spots indicates that mismatched relaxation between the Al_2O_3 and κ-Ga_2O_3 lattices occurred.

The transition layer was seen to consist of two components: α-Ga_2O_3 only two unit cells thick, connected directly to the substrate, and a 4−5 unit cells thick Ga_2O_3, with a previously unknown structure. The structure of the transition layer was studied by incoherent high-angle annular dark-field scanning transmission electron microscopy (HAADF-STEM) imaging along two different zone axes as shown in Figures 3a and S4, which provided structural and chemical information of the interface at the atomic level. The intensity of the atom columns in the HAADF-STEM image is approximately proportional to Z^2 where Z is the atomic number.[21] In the STEM images, the Ga^{3+} ion columns appear as bright dots, whereas the contrast of oxygen is too low to distinguish, as shown in Figure S5. The initial two layers of Ga_2O_3 have the same atomic configuration as that of the Al_2O_3 substrate along both the [100] and $[1\bar{1}0]$ zone axes. The phase was thus identified as an α-Ga_2O_3 phase, which has the same space group with α-Al_2O_3. No defects such as misfit dislocations could be found in the interface, implying that the α-Ga_2O_3 was under elastic strain with the substrate. Since the interface of α-Ga_2O_3/α-Al_2O_3 was sharp and defect free, it can be deduced that the α-Ga_2O_3 layers were fully strained, thus its in-plane parameters might be closer to those of α-Al_2O_3 phase.

Above the two unit cells of the α-Ga_2O_3 layer, there is an intermediate layer. The arrangement of Ga^{3+} ions in this layer as inferred by the image does not fit any of the known Ga_2O_3 phases. By DFT calculations, the structure of the intermediate layer was determined by invoking known A_2O_3 prototypes. The structure matched to the observed STEM image was identified as a disordered spinel phase (with the coordinates listing in Table 2). The illustration of the atomic structure of the few-layer interface is shown in Figure 3b.

Above the intermediate layer, the major Ga_2O_3 thin-film phase was identified as κ-Ga_2O_3 (as illustrated in Figure 3b), in agreement with the results obtained with electron diffraction.

DOI: 10.1021/acsami.8b17731
ACS Appl. Mater. Interfaces 2019, 11, 5536−5543

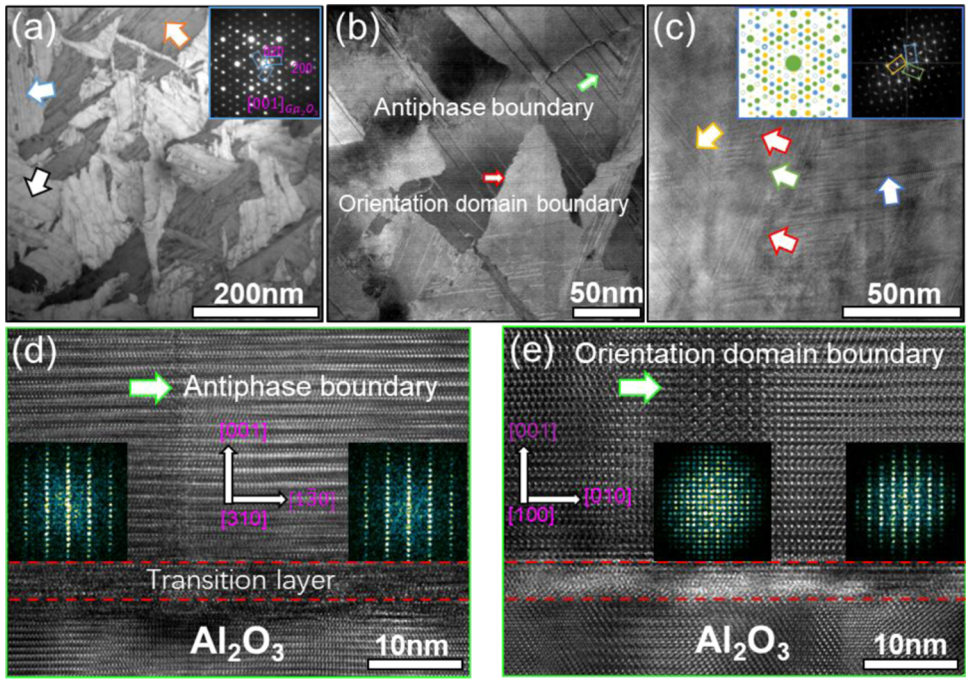

Figure 4. Plane-view TEM images of the Ga_2O_3/Al_2O_3 film viewed along the [001] zone axis of Al_2O_3. (a) Low-magnification bright-field TEM image of the Ga_2O_3/Al_2O_3 film, showing different contrasts of irregularly shaped domains in Ga_2O_3 film. Corresponding selected area diffraction patterns are shown as the inset indicating that they are orientation domains. (b) High-magnification bright-field TEM image of the Ga_2O_3/Al_2O_3 film system showing that there are many antiphase boundaries in each orientation domain. (c) Atomic resolution TEM image of the Ga_2O_3/Al_2O_3. The insert on the right is an fast Fourier transform (FFT) of the image, and the insert on the left is the simulated electron diffraction of the rotation domains. Cross-sectional high-resolution electron microscopy images of the Ga_2O_3/Al_2O_3 interface viewed along the (d) $[310]_{\kappa\text{-}Ga_2O_3}$and (e) $[100]_{\kappa\text{-}Ga_2O_3}$ zone axes, showing the antiphase boundary and orientation domain boundary.

There are many boundaries and defects in the κ-Ga_2O_3, as shown in Figure 1a. The κ-Ga_2O_3 phase was also studied along a plane-view (normal to the thin film) direction to characterize its overall architecture and defects, as shown in Figure 4. Obvious domain structures can be seen in Figure 4a, a bright-field image of the plane-view sample. Three sets of domain lines as indicated by three arrows were observed, and the angle among those lines was around 120°. The inset is a diffraction pattern acquired from the κ-Ga_2O_3, indicating that those domains are orientation domains, and the rotational angle among the domains is 120°. Figure 4b is a higher magnification image clearly showing orientation domain boundary (indicated by red arrow) and antiphase boundaries (indicated by green arrow). The size of the domains ranges from few nanometer to 200 nm.

The orientation domain boundaries are not straight and regular. Figure 4c is an atomic resolution image showing the domain and antiphase boundaries. As indicated by yellow, green, and blue arrows, the antiphase boundaries are parallel to the (100) plane of Ga_2O_3, and the orientation domain boundaries indicated by red arrows are parallel to the (110) plane of Ga_2O_3. To clearly display each orientation domain, inversed FFT reconstructions of Figure 4c are produced by keeping only the Fourier components related to a single domain region. These are shown in Figure S6 in which each rotational domain gains bright contrast in Figure S6a−c. The antiphase and domain boundaries can also be observed in the cross-sectional projection, as shown in Figure 4d,e. Figure 4d,e is cross-sectional atomic resolution TEM images acquired from the [310] and [100] zone axes of the Ga_2O_3 thin film, respectively. Along the cross-sectional direction, the domain boundaries have a wide overlapped region, unlike that of an antiphase boundary. The antiphase boundary can be identified in Figure 4d, whereas the orientation domain boundary with an obvious overlap area can be identified in Figure 4e. The relationship between the κ-Ga_2O_3 orientation domains and the α-Al_2O_3 substrate is shown in Figure 5. As the α-Al_2O_3 substrate has a hexagonal structure, it is not surprising to have 3-fold orientation domains in κ-Ga_2O_3.

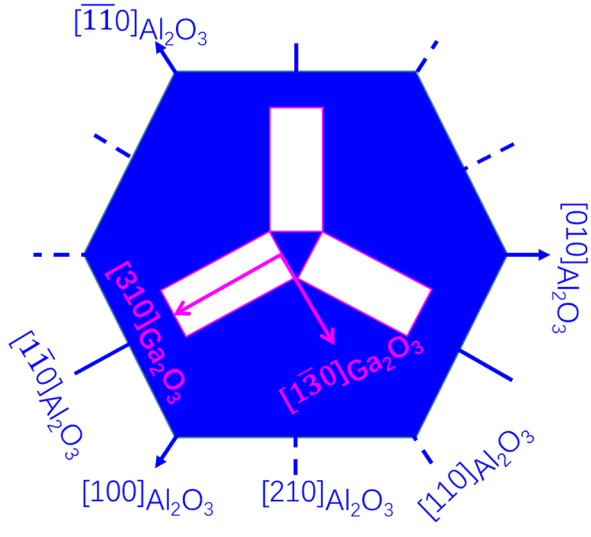

Figure 5. Schematic of the orientation configuration of κ-Ga_2O_3 orientation domains on the Al_2O_3(001) plane.

DOI: 10.1021/acsami.8b17731
ACS Appl. Mater. Interfaces 2019, 11, 5536−5543

On the basis of the structures of the interface phases, the mechanism of misfit strain release can now be better understood. The mismatch between α-Al_2O_3 and κ-Ga_2O_3 can be expressed in three directions: in-plane $[1\bar{3}0]_{\kappa\text{-}Ga_2O_3}//[110]_{Al_2O_3}$, in-plane $[310]_{\kappa\text{-}Ga_2O_3}//[1\bar{1}0]_{Al_2O_3}$, and out-of-plane $[001]_{\kappa\text{-}Ga_2O_3}//[001]_{Al_2O_3}$. The theoretical misfit along the in-plane $[1\bar{3}0]_{\kappa\text{-}Ga_2O_3}$ is −6.66%, along the in-plane $[310]_{\kappa\text{-}Ga_2O_3}$ is −19.74%, and along the out-of-plane $[001]_{\kappa\text{-}Ga_2O_3}$ is −8.28%. It is thus clear that the as-grown film would be under compressive and anisotropic in-plane strains imposed by the Al_2O_3 substrate. Such a large misfit cannot be simply relaxed by one interface. It is well known that the misfit dislocations are an important mechanism to relax strains between film and substrate.[27−29] However, no misfit dislocations could be found in the current study.

Using the phases identified, the theoretical mismatches in each interface are listed in Table 2. The few-layer α-Ga_2O_3 phase directly on the α-Al_2O_3 substrate is under elastic strain and thus can relax the misfit, estimated as about ∼4.5% along the in-plane directions and about ∼3.29% along the out-of-plane direction, as listed in Table 2. Above the α-Ga_2O_3 phase, there are some layers of intermediate phase which can also release some of the misfit. This changes the mismatch between α-Ga_2O_3 and κ-Ga_2O_3 along in-plane direction ([010]) to only about −1.93%. In addition, there are many domains and antiphase boundaries in the κ-Ga_2O_3 film that can also accommodate the rest of the misfit strain.

Experimental mismatch f_E can be derived based on experimental EDP, as shown in Figure 2a. f_E along the out-of-plane direction (κ-$Ga_2O_3[001]$) is around −6.95% and along the in-plane direction (κ-$Ga_2O_3[1\bar{3}0]$) is around −5.56%, both of which are slightly smaller than the theoretical value. By carefully calibrating the $(060)_{\kappa\text{-}Ga_2O_3}$ spot with the $(030)_{Al_2O_3}$ spot (Figure 2b), the experimental mismatch relaxation in κ-Ga_2O_3 is calculated to be ∼81.82%. In other words, the κ-Ga_2O_3 thin film is still under about ∼18.18% misfit strain caused by misfit imposed by the Al_2O_3 substrate. This is possibly the reason why the unstable phases become stable at room temperature but under such spatial and dimensional constraints.

By exploring the structures of the several Ga_2O_3, it appears that the ratio of octahedrally occupied Ga^{3+} ions and tetrahedrally occupied Ga-ions may affect the crystalline volume, and thus this ratio may provide a rationale for accommodating the misfit strain. In regard to the oxygen sublattice, whenever more oxygen tetrahedra are formed, the crystalline volume expands; from α-Ga_2O_3, cubic Ga_2O_3 to κ-Ga_2O_3, the oxygen tetrahedra increase gradually as the compressive strains imposed by the substrate become smaller and smaller from the substrate to the film. However, there is still ∼19% misfit strain left in the κ-Ga_2O_3 film, which prevents the formation of more oxygen-tetrahedrons. The stable Ga_2O_3 form, β-Ga_2O_3, has ∼50% oxygen forming tetrahedra, whereas in the unstable κ-Ga_2O_3 phase there are only ∼25% oxygen forming tetrahedra. Due to the remaining compressive strain, there must be more oxygen octahedrons to form a compact structure, leading to the stabilization of the phase (epitaxial stabilization).

CONCLUSIONS

In summary, the phase and interface structure of Ga_2O_3/Al_2O_3 have been carefully studied along different orientations via atomic resolution electron microscopy to reveal the mechanism of misfit match release. Due to the misfit strain and existence of a few-layer intermediate structure, the unstable κ-Ga_2O_3 has been found to become a stable phase in the film grown by the MOCVD method at 690°. The epitaxial stabilization appears to correlate with the tuning of the ratio of oxygen octahedra and tetrahedra (thus, also octahedrally or tetrahedrally coordinated Ga^{3+} ions). The crystalline volume can thus be tuned in this way to accommodate or match the externally applied strain caused by the mismatch between the substrate and film. Epitaxial growth can be applied to synthesize unstable structures due to the impact of the substrate, i.e., strain caused by lattice misfit. This work demonstrates that epitaxial engineering can be a promising method for preparing unstable and novel structures if the misfit strain can be better controlled.

METHODS/EXPERIMENTAL SECTION

Ga_2O_3 Preparation. The Ga_2O_3 thin film was grown on *c*-sapphire (0001) at 690 °C using a commercial metal organic chemical vapor deposition (MOCVD) method. Trimethylgallium (TMGa) and water were used as Ga and oxygen precursors, respectively, whereas H_2 was used as a carrier gas.[25]

TEM Sample Preparation. Cross-sectional TEM specimen was prepared by an FEI Helios NanoLab focused ion beam system. A plane-view sample was prepared by the conventional method including cutting, grinding, dimpling, and finally ion-milling. A Gatan 656 Dimple Grinder was used for dimpling. Ar ion-milling was performed by using a Gatan 691 Precision Ion Polishing System. The sample was thinned and ion-milled only from the Al_2O_3 substrate side until the Ar ion beam perforated the samples.

Structural Characterization. Electron diffraction patterns (EDPs) and diffraction contrast images were taken from a Hitachi H-8100 transmission electron microscope (TEM). A JEOL Grand ARM-300CF TEM equipped with high-angle annular dark-field (HAADF) detector, bright-field (BF) detector, annular bright-field (BF) detector, X-ray energy-dispersive spectrometer (EDS) systems operated at 300 kV was used for high-resolution images and EDS analysis. A JEOL ARM-200CF with probe aberration corrector was used for high-angle annular dark-field scanning transmission electron microscopy (HAADF-STEM) images. The beam convergence angle is around 20 mrad, and the collection angle ranging from 68 to 280 mrad. EDPs were simulated by SingleCrystal software.

First-Principles Calculations. All of the DFT calculations reported in this conducted experiment via the Vienna ab initio simulation package with the projector augmented wave potentials.[26−30] The Perdew−Burke−Ernzerhof[31] functional was used to deal with the exchange correlation. A plane wave basis with a cutoff energy of 520 eV and Γ-centered *k*-meshes with a density of 8000 *k*-points per reciprocal atom were used for all calculations. The Heyd−Scuseria−Ernzerhof screened hybrid functional (HSE06)[32−35] was used to accurately determine the electronic states of Ga and O in the phases.[37−39] To determine the structure of the transition phase of Ga_2O_3, prototype structures of A_2O_3, distinct from known Ga_2O_3 phases, including Al_2O_3 ($Fm\bar{3}m$,[22] $I4_1/amd$[36]), Fe_2O_3 ($P12_1/n1$,[40] $P4_12_12$,[41] $Aba2$[42]), were used with the corresponding Ga_2O_3 structures obtained through the DFT relaxation. The special quasi-random structure method[43−45] was used to generate structures for the disordered phases.

DOI: 10.1021/acsami.8b17731
ACS Appl. Mater. Interfaces 2019, 11, 5536−5543

■ ASSOCIATED CONTENT

Supporting Information

The Supporting Information is available free of charge on the ACS Publications website at DOI: 10.1021/acsami.8b17731.

Experimental and simulated EDPs; orientation relationship between different phases; high-resolution (S)TEM images and line profile along Ga_2O_3/Al_2O_3 interface (PDF)

■ AUTHOR INFORMATION

Corresponding Authors

*E-mail: wujs@whut.edu.cn (J.W.).
*E-mail: v-dravid@northwestern.edu (V.P.D.).

ORCID

Yaobin Xu: 0000-0002-9945-3514
Zhenpeng Yao: 0000-0001-8286-8257
Chris Wolverton: 0000-0003-2248-474X
Jinsong Wu: 0000-0002-7305-7927
Vinayak P. Dravid: 0000-0002-6007-3063

Present Addresses

[⊥]Department of Chemistry and Chemical Biology, Harvard University, 12 Oxford Street, Cambridge, Massachusetts 02138, United States (Z.Y.).
[∥]State Key Laboratory of Advanced Technology for Materials Synthesis and Processing, Nanostructure Research Centre, Wuhan University of Technology, Wuhan 430070, China (J.W.).

Notes

The authors declare no competing financial interest.

■ ACKNOWLEDGMENTS

Y.X. and J.W. (TEM and interpretation), Z.Y. and C.W. (DFT calculations), J.-H.P. and M.R. (sample preparation), and V.P.D. (TEM interpretation). This work made use of the EPIC facility of Northwestern University's NUANCE Center, which has received support from the Soft and Hybrid Nanotechnology Experimental (SHyNE) Resource (NSF NNCI-1542205); the MRSEC program (NSF DMR-1720139) at the Materials Research Center; the International Institute for Nanotechnology (IIN); the Keck Foundation; and the State of Illinois, through the IIN.

■ REFERENCES

(1) Langjahr, P. A.; Lange, F. F.; Wagner, T.; Ruhle, M. Lattice Mismatch Accommodation in Perovskite Films on Perovskite Substrates. *Acta Mater.* **1998**, *46*, 773−785.
(2) Gorbenko, O. Y.; Samoilenkov, S. V.; Graboy, I. E.; Kaul, A. R. Epitaxial Stabilization of Oxides in Thin Films. *Chem. Mater.* **2002**, *14*, 4026−4043.
(3) Norton, D. P. Synthesis and Properties of Epitaxial Electronic Oxide Thin-Film Materials. *Mater. Sci. Eng., R* **2004**, *43*, 139−247.
(4) Schlom, D. G.; Chen, L. Q.; Pan, X. Q.; Schmehl, A.; Zurbuchen, M. A. A Thin Film Approach to Engineering Functionality into Oxides. *J. Am. Ceram. Soc.* **2008**, *91*, 2429−2454.
(5) Stepanov, S. I.; Nikolaev, V. I.; Bougrov, V. E.; Romanov, A. E. Gallium Oxide: Properties and Applications - a Review. *Rev. Adv. Mater. Sci.* **2016**, *44*, 63−86.
(6) Higashiwaki, M.; Jessen, G. H. Guest Editorial: The Dawn of Gallium Oxide Microelectronics. *Appl. Phys. Lett.* **2018**, *112*, No. 060401.
(7) Li, L. D.; Wei, W.; Behrens, M. Synthesis and Characterization of α-, β-, and γ-Ga_2O_3 Prepared from Aqueous Solutions by Controlled Precipitation. *Solid State Sci.* **2012**, *14*, 971−981.
(8) Zheng, B.; Hua, W. M.; Yue, Y. H.; Gao, Z. Dehydrogenation of Propane to Propene over Different Polymorphs of Gallium Oxide. *J. Catal.* **2005**, *232*, 143−151.
(9) Higashiwaki, M.; Sasaki, K.; Kuramata, A.; Masui, T.; Yamakoshi, S. Gallium Oxide (Ga_2O_3) Metal-Semiconductor Field-Effect Transistors on Single-Crystal β-Ga_2O_3 (010) Substrates. *Appl. Phys. Lett.* **2012**, *100*, No. 013504.
(10) Hou, Y. D.; Wu, L.; Wang, X. C.; Ding, Z. X.; Li, Z. H.; Fu, X. Z. Photocatalytic Performance of α-, β-, and γ-Ga_2O_3 for the Destruction of Volatile Aromatic Pollutants in Air. *J. Catal.* **2007**, *250*, 12−18.
(11) Wang, X.; Xu, Q.; Li, M. R.; Shen, S.; Wang, X. L.; Wang, Y. C.; Feng, Z. C.; Shi, J. Y.; Han, H. X.; Li, C. Photocatalytic Overall Water Splitting Promoted by an Alpha-Beta Phase Junction on Ga_2O_3. *Angew. Chem., Int. Ed.* **2012**, *51*, 13089−13092.
(12) Eranna, G.; Joshi, B. C.; Runthala, D. P.; Gupta, R. P. Oxide Materials for Development of Integrated Gas Sensors - A Comprehensive Review. *Crit. Rev. Solid State Sci.* **2004**, *29*, 111−188.
(13) Kumaran, R.; Tiedje, T.; Webster, S. E.; Penson, S.; Li, W. Epitaxial Nd-doped Alpha-$(Al_{1-x}Ga_x)_2O_3$ Films on Sapphire for Solid-State Waveguide Lasers. *Opt. Lett* **2010**, *35*, 3793−3795.
(14) Zinkevich, M.; Aldinger, F. Thermodynamic Assessment of the Gallium-Oxygen System. *J. Am. Ceram. Soc.* **2004**, *87*, 683−691.
(15) Yoshioka, S.; Hayashi, H.; Kuwaabara, A.; Oba, F.; Matsunaga, K.; Tanaka, I. Structures and Energetics of Ga_2O_3 Polymorphs. *J. Phys.: Condens. Matter* **2007**, *19*, No. 346211.
(16) Playford, H. Y.; Hannon, A. C.; Barney, E. R.; Walton, R. I. Structures of Uncharacterised Polymorphs of Gallium Oxide from Total Neutron Diffraction. *Chem. - Eur. J.* **2013**, *19*, 2803−2813.
(17) Baroni, S.; de Gironcoli, S.; Dal Corso, A.; Giannozzi, P. Phonons and Related Crystal Properties from Density-Functional Perturbation Theory. *Rev. Mod. Phys.* **2001**, *73*, 515−562.
(18) Ahman, J.; Svensson, G.; Albertsson, J. A Reinvestigation of Beta-Gallium Oxide. *Acta Crystallogr., Sect. C: Cryst. Struct. Commun.* **1996**, *52*, 1336−1338.
(19) Pohl, K. Hydrothermic Formation of γ-Ga_2O_3. *Naturwissenschaften* **1968**, *55*, No. 82.
(20) He, H. Y.; Blanco, M. A.; Pandey, R. Electronic and Thermodynamic Properties of Beta-Ga_2O_3. *Appl. Phys. Lett.* **2006**, *88*, No. 261904.
(21) Cora, I.; Mezzadri, F.; Boschi, F.; Bosi, M.; Čaplovičová, M.; Calestani, G.; Dódony, I.; Pécza, B.; Fornari, R. The Real Structure of ε-Ga_2O_3 and Its Relation to Kappa-Phase. *CrystEngComm* **2017**, *19*, 1509−1516.
(22) Levin, I.; Brandon, D. Metastable Alumina Polymorphs: Crystal Structures and Transition Sequences. *J. Am. Ceram. Soc.* **1998**, *81*, 1995−2012.
(23) Playford, H. Y.; Hannon, A. C.; Tucker, M. G.; Dawson, D. M.; Ashbrook, S. E.; Kastiban, R. J.; Sloan, J.; Walton, R. I. Characterization of Structural Disorder in Gamma-Ga_2O_3. *J. Phys. Chem. C* **2014**, *118*, 16188−16198.
(24) Binet, L.; Gourier, D.; Minot, C. Relation between Electron Band-Structure and Magnetic Bistability of Conduction Electrons in β-Ga_2O_3. *J. Solid State Chem.* **1994**, *113*, 420−433.
(25) Razeghi, M.; Park, J. H.; McClintock, R.; Pavlidis, D.; Teherani, F. H.; Rogers, D. J.; Magill, B. A.; Khodaparast, G. A.; Xu, Y. B.; Wu, J. S.; Dravid, V. P. A Review of the Growth, Doping, and Applications of β-Ga_2O_3 Thin Films. *Proc. SPIE* **2018**, *10533*, No. 105330R, DOI: 10.1117/12.2302471.
(26) Pennycook, S. J.; Boatner, L. A. Chemically Sensitive Structure-Imaging with a Scanning-Transmission Electron-Microscope. *Nature* **1988**, *336*, 565−567.
(27) Fornari, R.; Pavesi, M.; Montedoro, V.; Klimm, D.; Mezzadri, F.; Cora, I.; Pécze, B.; Boschi, F.; Parisini, A.; Baraldi, A.; Ferrari, C.; Gombia, E.; Bosi, M. Thermal Stability of ε-Ga_2O_3 Polymorph. *Acta Mater.* **2017**, *140*, 411−416.

DOI: 10.1021/acsami.8b17731
ACS Appl. Mater. Interfaces 2019, 11, 5536−5543

(28) Suzuki, T.; Nishi, Y.; Fujimoto, M. Analysis of Misfit Relaxation in Heteroepitaxial $BaTiO_3$ Thin Films. *Philos. Mag. A* **1999**, *79*, 2461−2483.
(29) Xu, Y. B.; Tang, Y. L.; Zhu, Y. L.; Liu, Y.; Li, S.; Zhang, S. R.; Ma, X. L. Misfit Strain Relaxation of Ferroelectric $PbTiO_3/LaAlO_3$ (111) Thin Film System. *Sci. Rep.* **2016**, *6*, No. 35172.
(30) Blöchl, P. E. Projector Augmented-Wave Method. *Phys. Rev. B* **1994**, *50*, 17953−17979.
(31) Kresse, G.; Hafner, J. Ab Initio Molecular Dynamics for Liquid Metals. *Phys. Rev. B* **1993**, *47*, 558−561.
(32) Kresse, G.; Hafner, J. Ab-Initio Molecular-Dynamics Simulation of the Liquid-Metal Amorphous-Semiconductor Transition in Germanium. *Phys. Rev. B* **1994**, *49*, 14251−14269.
(33) Kresse, G.; Furthmüller, J. Efficiency of Ab-Initio Total Energy Calculations for Metals and Semiconductors Using a Plane-Wave Basis Set. *Comput. Mater. Sci.* **1996**, *6*, 15−50.
(34) Kresse, G.; Furthmüller, J. Efficient Iterative Schemes for Ab Initio Total-Energy Calculations Using a Plane-Wave Basis Set. *Phys. Rev. B* **1996**, *54*, 11169−11186.
(35) Perdew, J. P.; Ernzerhof, M.; Burke, K. Rationale for Mixing Exact Exchange with Density Functional Approximations. *J. Chem. Phys.* **1996**, *105*, 9982−9985.
(36) Heyd, J.; Scuseria, G. E.; Ernzerhof, M. Hybrid Functionals Based on a Screened Coulomb Potential. *J. Chem. Phys.* **2003**, *118*, 8207−8215.
(37) Li, Q.; Liu, H.; Yao, Z.; Cheng, J. P.; Li, T. H.; Li, Y.; Wolverton, C.; Wu, J.; Dravid, V. P. Electrochemistry of Selenium with Sodium and Lithium: Kinetics and Reaction Mechanism. *ACS Nano* **2016**, *10*, 8788−8795.
(38) Bin, H.; Yao, Z. P.; Zhu, S. M.; Zhu, C. L.; Pan, H.; Chen, Z. X.; Wolverton, C.; Zhang, D. A High-Performance Anode Material Based on $FeMnO_3$/Graphene Composite. *J. Alloys Compd.* **2017**, *695*, 1223−1230.
(39) Samain, L.; Jaworski, A.; Edén, M.; Ladd, D. M.; Seo, D. K.; Garcia-Garcia, F. J.; Häussermann, U. Structural Analysis of Highly Porous γ-Al_2O_3. *J. Solid State Chem.* **2014**, *217*, 1−8.
(40) Bykova, E.; Bykov, M.; Prakapenka, V.; Konôpková, Z.; Liermann, H. P.; Dubrovinskaia, N.; Dubrovinsky, L. Novel High Pressure Monoclinic Fe_2O_3 Polymorph Revealed by Single-Crystal Synchrotron X-ray Diffraction Studies. *High Pressure Res.* **2013**, *33*, 534−545.
(41) Jørgensen, J.-E.; Mosegaard, L.; Thomsen, L. E.; Jensen, T. R.; Hanson, J. C. Formation of γ-Fe_2O_3 Nanoparticles and Vacancy Ordering: An in Situ X-ray Powder Diffraction Study. *J. Solid State Chem.* **2007**, *180*, 180−185.
(42) Bykova, E.; Dubrovinsky, L.; Dubrovinskaia, N.; Bykov, M.; McCammon, C.; Ovsyannikov, S. V.; Liermann, H. P.; Kupenko, I.; Chumakov, A. I.; Rüffer, R.; Hanfland, M.; Prakapenka, V. Structural Complexity of Simple Fe_2O_3 at High Pressures and Temperatures. *Nat. Commun.* **2016**, *7*, No. 10661.
(43) Cockayne, E.; van de Walle, A. Building Effective Models from Sparse but Precise Data: Application to an Alloy Cluster Expansion Model. *Phys. Rev. B* **2010**, *81*, No. 012104.
(44) van de Walle, A. Methods for First-Principles Alloy Thermodynamics. *JOM* **2013**, *65*, 1523−1532.
(45) van de Walle, A. Multicomponent Multisublattice Alloys, Nonconfigurational Entropy and Other Additions to the Alloy Theoretic Automated Toolkit. *Calphad* **2009**, *33*, 266−278.

DOI: 10.1021/acsami.8b17731
ACS Appl. Mater. Interfaces 2019, 11, 5536−5543